

A target imaging method of multiple-input-multiple-output ground penetrating radar-based on direction of arrival estimation

Xi Jianjun^{1,2,*} and Huang Ling³

¹Powerchina Hebei Electric Power Design & Research Institute Co. LTD, Shijiazhuang 050031, China

²College of Exploration Science and Technology, Jilin University, Changchun 130026, China

³Institute of Electronics, Chinese Academy of Sciences, Beijing 100190, China

In this study we consider imaging of the multiple-input-multiple-output ground penetrating radar (MIMO-GPR) system, and analyse the effect and accuracy of the estimation for target echo arrival upon direction of arrival (DOA) in the three beam-forming algorithms, i.e. least square, Capon algorithm and amplitude phase estimation. We propose a method of multi-antenna GPR target imaging based on the DOA estimation. This method, to perform the target imaging, makes combined use of DOA estimation of target echo signal in MIMO array and array spatial observation information. By spatial scanning for the imaging points, the target is localized and the reflection intensity is estimated from the weighted integral of each estimated DOA amplitude value at the imaging point. This method, with simpler practice, less data observation frequency and more efficient calculation, can speed up the target detection measurement and improve the data interpretation efficiency.

Keywords: Beam-forming algorithms, direction of arrival estimation, ground penetrating radar, target imaging.

GROUND penetrating radar (GPR) is based on the reflection and scattering of high-frequency radio waves generated in the target medium. It is used to ascertain the target interior distribution regulations, locate, identify and image the target, and estimate its main physical parameters using related algorithm. The conventional GPR and imaging algorithms mostly use single-input-single-output (SISO). Several data processing and imaging algorithms have explored much of the SISO imaging potential and thus hardly has a further qualitative leap. Multiple-input-multiple-output (MIMO) is a new type of radar system developed in recent years. It reduces the effect of radar cross-section (RCS) angle fluctuations on the parameter estimation and improves detection performance and spatial resolution, by taking better advantage of the detection

system and target time-space domain data compared to SISO. Roberts *et al.*¹ applied an iteration adaptation method based on least square to realize MIMO imaging, and testified that the MIMO array Doppler and angular resolution was higher than the single-input-multiple-output array on comparing the images obtained from least square algorithms. Xu and Li² discussed the anti-jamming capability and resolution performance of adaptive techniques like Capon and amplitude phase estimation with or without array calibration errors using MIMO imaging, worked out in adaptive super-resolution spectral estimation. Tabrikian³ studied the Barankin limit in MIMO DOA estimation. Wang Juting *et al.*⁴ studied the Cramer-Rao bound in direction of arrival estimation in the compound Gaussian background. Wei and Zi Zhu⁵ studied the viability of amplitude phase estimation algorithm in MIMO parameter estimation. At the aspects of array antenna design, imaging model and imaging algorithm, learners have discussed about small airspace monitoring of ultra wide band (UWB) MIMO radio array, and applied the backward projection algorithm for obtaining an ideal point target imaging. Xing Bin *et al.*⁶ studied the distributed multichannel radar imaging in MIMO system, and developed the MIMO 2D imaging model for simple linear arrangement of the transmit-receive array collocation. A 3D broadband MIMO imaging model and corresponding 3D imaging algorithm were also developed by other researchers^{7,8}. Ji Yu⁹ performed target reconstruction by duality differential method to deal with the random disturbance of medium refractive index and minimized the computation amount.

The above-mentioned conventional single-antenna radar imaging techniques are simple to use and have been applied successively and widely in relative fields. However, due to the limited available information, they hardly improve the target positioning and space resolution in radar imaging. Though some imaging methods can overcome the above issues to a certain extent, they are still unable to eliminate the impact of weak interferences and errors upon imaging. Moreover, the bottlenecks in imaging

*For correspondence. (e-mail: tiantianhappy365@126.com)

technique, such as poor instantaneity and motion compensation, have not been settled yet^{10,11}. There are also many technical difficulties in GPR imaging, such as the single data processing, short effective detection range, low-resolution imaging, etc.¹². Besides, the conventional GPR antenna, restricted by the level of development of electronic devices, can hardly transmit an ideal, high-fidelity, ultra-narrow timewidth pulse signal. The target imaging location parameters are vague in single-point observation and recognition capability of the target spatial information is poor^{13,14}. Most migration methods for common offset usually assume that the antennas reflect and receive homogeneously in all directions, while ignore the fact radar cross-section changes with the electromagnetic incident angle and scattering angle, and the transmit-receive antenna pattern and radar cross-section have an influence on the migration imaging^{15,16}. Learners have been striving for solving the above defects in conventional single antenna imaging. However, the radar target detection performance and imaging resolution ratio are still not up to satisfaction, due to the complexity in application and algorithm as well as diversity in affecting factors and hypothesis. Therefore, there is an urgent need to develop a new technique for GPR imaging.

MIMO-GPR signal model is a type of target detection system based on narrow-band modulation signal and scattering point target model. The narrow-band modulation signal is taken as the target detection signal, and orthogonal modulation signal is used on each array antenna transmission element, so as to realize waveform diversity. Adaptive array beam-forming technique and inverse direction imaging method (IDIM) are adopted in data processing for imaging the target. Beam-forming technique can self-adapt to the weighting factors of each high-speed array element based on the changes of signal environment, thus can enhance the signal and suppress the interference.

A steady estimation for the DOA is the key to array signal processing, but in conventional array signal, it is restricted by the set quantity of array physical apertures and array elements. The orthogonal signal transmitted by MIMO radar, with its diversity characteristic, can extend the aperture after a series of processing, raise the degree of freedom geometrically, and consequently improve the performance of direction of arrival estimation. This article deals with the MIMO-GPR target imaging issue and brings forward a method of multi-antenna GPR detection target imaging based on DOA estimation.

MIMO-GPR signal model

Basic model of detection signal

The electromagnetic wave signals, which transmit at the transmit-receive antenna terminals and through underground medium of the MIMO-GPR, are high frequency

narrow-band modulation signals. Slight time delay will occur when the signals are transmitting from antennas at different spatial positions. The slight time delay is shown as a narrow-band signal phase shift; the narrow-band signal is commonly shown as an equivalent low-pass signal. The pass-band signal with centre frequency f_c is shown as¹⁷

$$r(t) = R\{s(t)e^{j2\pi f_c t + \theta_0}\}, \quad (1)$$

where $R\{\ast\}$ is the complex real number, and the baseband signal $s(t)$ is the complex envelope of the real signal $r(t)$, i.e. the equivalent low-pass signal and baseband modulation signal. Demodulate $r(t)$ to obtain $s(t)$ from the real observed signal, i.e. multiply both $\cos(2\pi f_c t)$ and $-\sin(2\pi f_c t)$ by $r(t)$, and then make low-pass filtering.

For the narrow-band signal, the signal time delay, if less than the reciprocal of the band width, is equivalent to the phase shift. The high-frequency modulation signal in narrow-band signal condition is

$$\begin{cases} x(t) = s(t)e^{-j2\pi f_c t}, \\ x(t-\tau) \approx x(t)e^{-j2\pi f_c \tau}. \end{cases} \quad (2)$$

Target detection model

Consider a multiple-input-multiple-output radar system with N_T number of transmitting and N_R number of receiving antennas. Let $\mathbf{s}(t)$ as the baseband signal transmitted from each transmitting antenna in the array. Let $s_m(t)$ be the scattered baseband signal of m transmitting antenna elements, which is modulated and transmitted by the carrier signal of angular frequency ω_0 .

The electromagnetic wave in spatial transmission is a 4D function of time and space as shown in Figure 1, where α is the direction of propagation of the electromagnetic wave in the transmitting array. The plane wave at the coordinate origin can be shown as the analytic signal as follows¹⁷

$$x_m(0, t) = s_m(t)e^{j\omega_0 t}. \quad (3)$$

In the narrow-band condition, the complex envelopes of the sampled signal in each array element in the spatial array are the same. The field value at the far field target location \mathbf{r} is

$$x_m(\theta_T, t) = s_m(t)e^{j\omega_0 \left(t - \frac{R_T}{v}\right)},$$

where R_T is the reference element distance from the target to the transmitting array element.

Assume the element N_T array antenna is a uniform linear array (ULA), and the spacing between adjacent

elements is d (Figure 2). Assuming that a scattering point target exists at θ_T and the target electromagnetic scattering coefficient is $\beta(\theta_T)$, the target scattering signal is

$$\beta(\theta_T)\xi_{R_r}x(t) = \xi_{R_r}\beta(\theta_T)\mathbf{a}^T(\theta_T)s(t). \quad (4)$$

The scattered signal at the scattering point is taken as the source signal of the receiving array antenna. θ_R is taken as the DOA estimation from the scattering point to the receiving array antenna beam arrival angle. If the transmitting and receiving antenna arrays are co-located or co-sharing, the scattering point is one and the same for the transmitting and receiving arrays thus $\beta(\theta_T) \equiv \beta(\theta_R)$. Assuming the reference element distance is R_R from the scattering point to the receiving array, the receiving signal for the reference antenna is

$$\begin{aligned} \mathbf{y}(t) &= \sum_{i=1}^P \mathbf{b}(\theta_{R_i})\xi_{R_{R_i}}\beta(\theta_{T_i})x_i(t) \\ &= \sum_{i=1}^P \mathbf{b}(\theta_{R_i})\xi_{R_{R_i}}\xi_{R_{T_i}}\beta(\theta_{T_i})\mathbf{a}^T(\theta_{T_i})s(t). \end{aligned} \quad (5)$$

For the more common non-uniform array antenna or array antenna with large element spacing, the difference between different system signal models lies in the difference between the array steering vectors. $\mathbf{a}(\theta_T)$ and $\mathbf{b}(\theta_R)$ are changed into the universal form as $\bar{\mathbf{a}}(\theta_T)$ and $\bar{\mathbf{b}}(\theta_R)$,

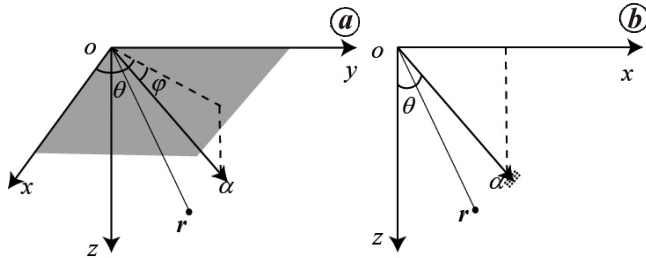


Figure 1. Array signal coordinate conventions. a, 3D; b, 2D.

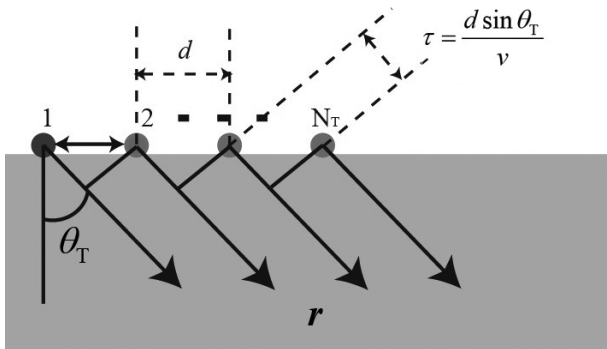


Figure 2. Geometry of isometric emission line array.

with parameters in Figure 3, of which R_T is the distance from the reference antenna to the target

$$\bar{\mathbf{a}}(\theta_T) = [1 \ e^{j\omega_0\tau_{T2}} \ e^{j\omega_0\tau_{T3}} \ \dots \ e^{j\omega_0\tau_{TN_T}}]^T, \quad (6)$$

$$\bar{\mathbf{b}}(\theta_R) = [1 \ e^{j\omega_0\tau_{R2}} \ e^{j\omega_0\tau_{R3}} \ \dots \ e^{j\omega_0\tau_{RN_R}}]^T. \quad (7)$$

The time shifting τ_{Tm} of the m antenna element relative to the reference antenna is

$$\tau_{Tm} = \frac{\sqrt{\left[\left| \sum_{i=2}^m d_i \right| - R_T \sin(\theta_T) \right]^2 + \left| R_T \cos(\theta_T) \right|^2} - R_T}{v}. \quad (8)$$

It follows that for the discontinuous array antennas or for antennas with large element spacing, the direction vector of the array signal is determined by the array element distribution parameter, DOA estimation of the target relative reference antenna arrival angle and target distance R . For target DOA estimation, besides obtaining DOA estimation by the method of scanning, the target distance R is also taken into account.

Target imaging method

In this article, the MIMO-GPR imaging method is divided into three steps as follows.

First, demodulate the transmitted baseband signal from the array signals by matched filtering, and estimate the range delay τ between the array and the target.

Secondly, perform direction of arrival estimation based on beam former, and estimate the target response amplitude and phase (AP).

Thirdly, scan the imaging space and perform target imaging based on τ , DOA estimation of target response arrival angle as well as AP.

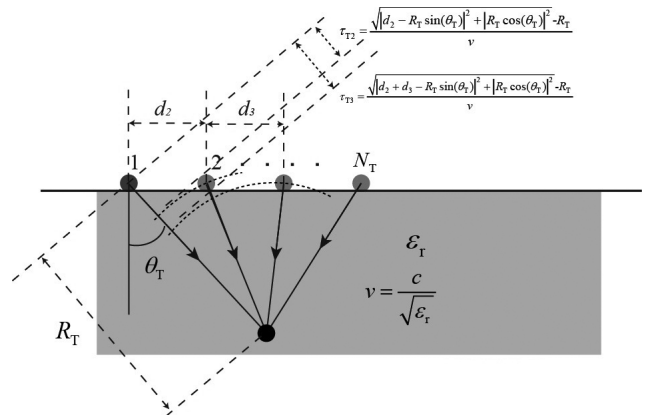


Figure 3. Generalized transmitting antenna array.

The target imaging information is obtained in two ways, i.e. from the orthogonally obtained amplitude information of each transmitting antenna element and from the phase information of the narrow-band carrier signal displayed on the array.

The design for MIMO-GPR detection process includes the following.

- (1) For those beams transmitted mutually independently or with orthorhombic detection information, which have their half-space radiating antenna array defined, design the corresponding beam-forming weight coefficient.
- (2) Select the appropriate carrier according to the geological conditions, working environment and interference source characteristic.
- (3) Make in-phase quadrature demodulation for the array signal, estimate the target range delay through matched filtering, and receive the array baseband signal.
- (4) Carry out DOA estimation using beam former estimation method or any alternative adaptive array signal processing technique and estimate the target amplitude.
- (5) Perform target imaging by utilizing the target response signal direction of arrival, target signal amplitude and range delay.

Target DOA estimation methods

The array signal model

$$\mathbf{Y} = \mathbf{b}^*(\theta)\beta(\theta)\mathbf{a}^H(\theta)\mathbf{S} + \mathbf{Z}, \quad (9)$$

where $\mathbf{S} = [\mathbf{s}(1) \ \mathbf{s}(2) \ \dots \ \mathbf{s}(N)]$ is the transmitting baseband signal and $\mathbf{Y} \in \mathbb{C}^{N_r \times N}$ is the receiving signal matrix $\beta(\theta)$ is the complex amplitude of the reflected signal in θ direction, directly proportional to the radar cross-section of the target in the same direction. $\mathbf{Z} \in \mathbb{C}^{N_r \times N}$ is the residual term including noise and disturbance¹⁷. The question is how to estimate the amplitude value $\beta(\theta)$ of all target signals at the angle θ from the receiving signal \mathbf{Y} and form a spatial spectrum accordingly.

The signal model developed here omits the time of arrival (TOA, τ) of the target signal. Nevertheless, the unknown condition of the target echo signal arrival time τ is not difficult to be included in eq. (9). By estimating τ and $\beta(\theta)$ employing current methods, 2D radar detection image can be developed. The MIMO-GPR inverse direction imaging method estimates DOA only from the array signal. The target distance is imaged from direction of arrival estimation and obtained from multiple observation results in different locations. The target location or distance parameters are determined by the geometrical relationship of multiple DOA estimations instead of obtaining directly from time of arrival.

The basic principle of the adaptive beam-forming is to make the beam maximum value point to the target direction while trying to suppress the interference and noise. This is equivalent to minimizing the total output power in beam-forming under a certain guaranteed signal power.

The common framework of the adaptive beam-forming is illustrated mathematically as a constrained quadratic optimization issue

$$\begin{cases} \min \{W^H R_{xx} W\}, \\ \text{s.t. } f(W) = 0, \end{cases} \quad (10)$$

where $W \in \mathbb{C}^{M_r \times 1}$ is the weight vector of the airspace filter to suppress the noise and interference, and to maintain the signal undistorted. R_{yy} is the covariance matrix of the observed signal sampling (N as the sampling count)

$$R_{yy} = \frac{1}{N} \mathbf{Y} \mathbf{Y}^H. \quad (11)$$

The DOA is estimated by three optimized beam-forming algorithms, i.e. least square, Capon algorithm and amplitude phase estimation.

- (1) Least square: This proceeds as follows^{18,19}

$$\beta_{\text{DAS}}(\theta) = \frac{b^T(\theta) \mathbf{Y} \mathbf{S}^H a(\theta)}{N \|\mathbf{b}(\theta)\|^2 (a^H(\theta) R_{xx} a(\theta))} \quad (12)$$

where $\|\cdot\|^2$ is the Euclidean distance norm, \mathbf{Y} the transmitting and receiving signal matrix respectively, $a(\theta)$ and $b(\theta)$ the steering vector of the transmitting and receiving array respectively, R_{xx} the covariance matrix of the transmitting signal, $[\cdot]^T$ and $[\cdot]^*$ are the transpose and complex conjugate of the matrix respectively.

- (2) Capon algorithm: Capon beam former is used to carry out the following constraint optimization²⁰, divided into two steps, viz. step-1 Capon beam-forming and step-2 realizing least square estimation by matched filtering

$$\min \{W^H R_{yy} W\} \quad \text{s.t.} \quad W^H \mathbf{b}^*(\theta) = 1. \quad (13)$$

The output of Capon beam-formings

$$\frac{\mathbf{b}^T(\theta) R_{yy}^{-1} \mathbf{Y}}{\mathbf{b}^T(\theta) R_{yy}^{-1} \mathbf{b}^*(\theta)}. \quad (14)$$

Substituting the above into signal model formula, i.e. eq. (9), we get

$$\frac{\mathbf{b}^T(\theta) R_{yy}^{-1} \mathbf{Y}}{\mathbf{b}^T(\theta) R_{yy}^{-1} \mathbf{b}^*(\theta)} = \beta(\theta) \mathbf{a}^*(\theta) \mathbf{S} + \frac{\mathbf{b}^T(\theta) R_{yy}^{-1} \mathbf{Z}}{\mathbf{b}^T(\theta) R_{yy}^{-1} \mathbf{b}^*(\theta)} \quad (15)$$

We estimate the output of the beam former $W_{\text{Capon}}^H \mathbf{Y}$ by the least square method. The spatial spectrum can be estimated^{21,22}

$$\beta_{\text{Capon}}(\theta) = \frac{\mathbf{b}^H(\theta)R_{yy}^{-1}R_{ys}^{-1}a(\theta)}{N(\mathbf{b}^H(\theta)R_{yy}^{-1}b^*(\theta))(a^H(\theta)R_{ss}^{-1}a(\theta))} \quad (16)$$

where

$$R_{ss} = \frac{1}{N}SS^H, \quad R_{yy} = \frac{1}{N}YY^H, \quad R_{ys} = \frac{1}{N}YX^H, \quad (17)$$

are the transmitting signal, receiving signal and covariance matrix respectively. Equation (16) is obviously a θ function, and one spatial spectrum can be obtained by calculating each θ value in eq. (16).

(3) Amplitude phase estimation algorithm: This is a non-parametric spectral analysis method, having high estimation precision but with computational complexity. It can be illustrated as a constraint optimization issue as below

$$\min \{ \|W^H Y - \beta(\theta)a^T(\theta)S\|^2 \} \quad \text{s.t. } W^H b(\theta) = 1. \quad (18)$$

Expanding the objective function

$$\begin{aligned} \|W^H Y - \beta a^T(\theta)X\|^2 &= W^H R_{yy}^{-1}W - \beta W^H R_{ys}^{-1}a^*(\theta) \\ &\quad - \beta a^T(\theta)R_{ys}^H W + |\beta|^2 a^T(\theta)R_{ss}^H W a^*(\theta) \\ &= \left(\beta - \frac{W^H R_{ys} a^*(\theta)}{a^T(\theta)R_{ss} a^*(\theta)} \right) a^T(\theta)R_{ss} a^*(\theta) \left(\beta - \frac{W^H R_{ys} a^*(\theta)}{a^T(\theta)R_{ss} a^*(\theta)} \right) \\ &\quad + W^H \left(R_{yy} - \frac{R_{ys} a^*(\theta)a^T(\theta)R_{ys}^H}{a^T(\theta)R_{ss} a^*(\theta)} \right) W. \end{aligned} \quad (19)$$

Using the above equation, the $\beta(\theta)$ can be estimated

$$\beta(\theta) = \frac{W^H R_{ys} a^*(\theta)}{a^T(\theta)R_{ss} a^*(\theta)}. \quad (20)$$

Substituting the above into eq. (19), the optimization issue can be rewritten as

$$\min \{ \|W^H Q W\|^2 \} \quad \text{s.t. } W^H \mathbf{b}(\theta) = 1, \quad (21)$$

where the estimation of the noise covariance matrix is estimated as

$$Q = R_{yy} - \frac{R_{ys} a^*(\theta)a^T(\theta)R_{ys}^H}{a^T(\theta)R_{ss} a^*(\theta)}. \quad (22)$$

Solving the above equation, the weight vector of the amplitude phase estimation airspace filter can be worked out.

$$W_{\text{APES}} = \frac{Q^{-1} \mathbf{b}(\theta)}{\mathbf{b}^H(\theta)Q^{-1} \mathbf{b}(\theta)}. \quad (23)$$

Substituting the above into eq. (20), the echo complex amplitude $\beta_{\text{APES}}(\theta)$ is estimated

$$\beta_{\text{APES}}(\theta) = \frac{a^H(\theta)Q^{-1}R_{ys} a^*(\theta)}{(\mathbf{b}^H(\theta)Q^{-1} \mathbf{b}^*(\theta))(a^H(\theta)R_{ss} a^*(\theta))}, \quad (24)$$

$$R_{yy} = \frac{1}{N} \mathbf{Y} \mathbf{Y}^H. \quad (25)$$

Comparison of three DOA spectral estimation methods

The MIMO radar detection model simulation was used to analyze DOA spectral estimation performance of different parameters. If the background dielectric constant $\epsilon_r = 9$, the carrier frequency $f_0 = 0.1$ GHz, then the carrier propagation velocity

$$v = \frac{c}{\text{sqrt}(\epsilon_r)} = \frac{0.3}{\text{sqrt}(9)} = 0.1 \text{ m/ns},$$

wavelength

$$\lambda_0 = \frac{v}{f_0} = \frac{0.1}{0.1} = 1 \text{ m}.$$

and the number of elements of the transmit-receive co-located uniform linear array $N_T = N_R = 6$. Figure 4 depicts the detection model. The number of array antenna (Ant_Num) is 6 and the element spacing (Ant_Spc) is 0.5 m, while the signal-to-noise ratio (SNR) changes within the range of 10 to -25 dB.

When the array (no. 1 antenna element) is at the 0 m coordination position of the model, the DOA of point target to the array arrival angle is 45°. In Figure 5, the angular resolutions of the three DOA spectral estimations in the single target model are compared. It is observed that the three methods have the same amplitude estimation precision, but are greatly different in angular resolution. The direction of arrival angular resolution is high to low in Capon algorithm, amplitude phase estimation and least square respectively.

Figure 6 shows the comparisons of DOA estimation in the three methods when the SNR changes within the range 10 to -25 dB. It is observed that the results are basically the same in low SNR condition. When the SNR is lower than -20 dB, large side beam arises in all the

three methods, which causes false target or impairs the imaging capacity at the target position. In the target direction, estimation precision in least square is scarcely relevant to the SNR. In Capon algorithm, direction of arrival estimation has high precision in high SNR condition, but its angular estimation precision is lowered along with the reduction of SNR. The estimation performance of amplitude phase estimation is between that of least square and Capon.

Figure 7 shows DOA estimation in the three methods for different (Ant_Spc)s. The number of array antenna (Ant_Num) is 6 and the element spacing (Ant_Spc) changes within the range $\lambda_0/2$ to $\lambda_0/10$. It is observed that in the Capon algorithm, estimation maintains high precision and stability and angular resolution maintains a high level in small antenna spacing. In the least square, the precision of estimation lowers promptly along with the lessening of spacing, even too difficult to work out when the spacing is so small; moreover, the sidelobe oscillation in least square is more obvious. To sum up, in both Capon and amplitude phase estimation methods, DOA estimation is highly stable, without sidelobe oscillation arising.

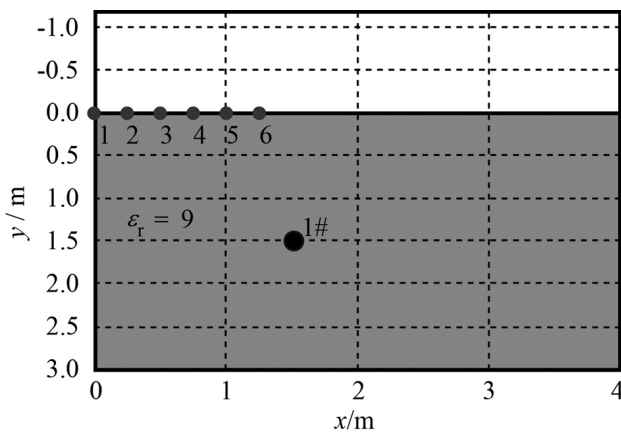


Figure 4. Single target model.

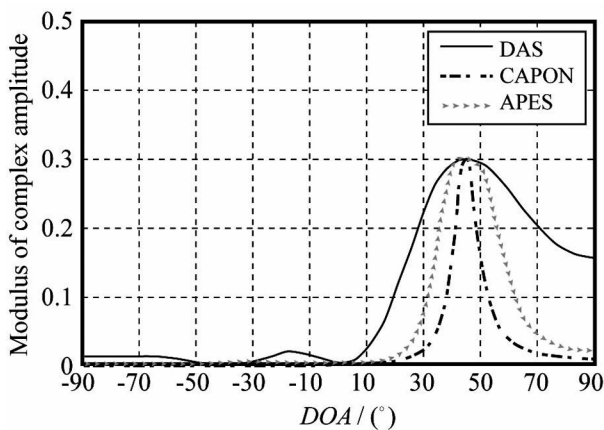


Figure 5. Comparison of $\beta(\theta)$ in three direction of arrival methods.

Figure 8 shows DOA estimation in the three methods when Ant_Spc is invariant and Ant_Num is changed. Ant_Num changes from MIMO (2, 2) to MIMO (12, 12). It is observed that if Ant_Num is as small as 2, no matter by using any of the three methods, it can neither estimate DOA nor distinguish the target direction. However, when Ant_Num is equal to or more than 4, DOA can be estimated using all three methods. The estimation precision is similar in amplitude phase estimation and Capon and is slightly inferior in least square.

Figure 9 makes a profiling observation, which is similar to that in conventional impulse ground radar, to measure the radar antenna array repeatedly along the horizontal direction and estimate DOA of the target using

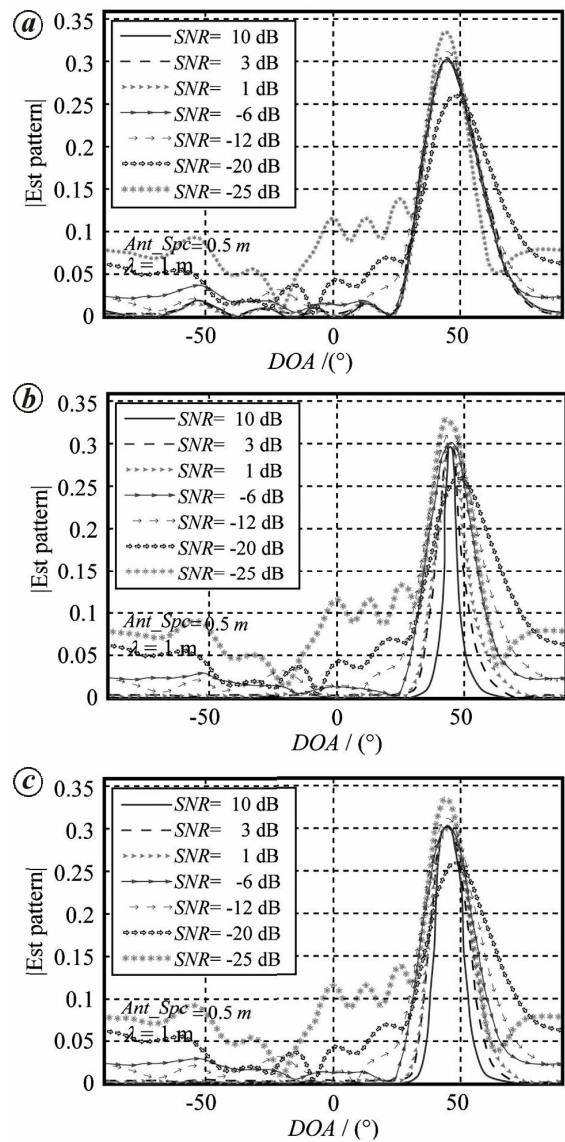


Figure 6. Relationship between $\beta(\theta)$ and signal-to-noise ratio in three direction of arrival methods. *a*, Least square; *b*, Capon; *c*, amplitude phase estimation.

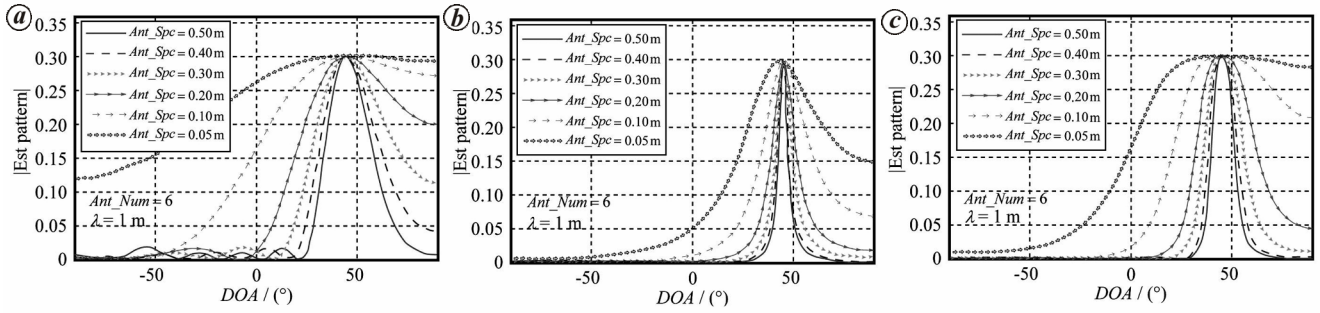


Figure 7. Relationship between $\beta(\theta)$ and (Ant_Spc) in three direction of arrival methods. *a*, Least square; *b*, Capon; *c*, amplitude phase estimation.

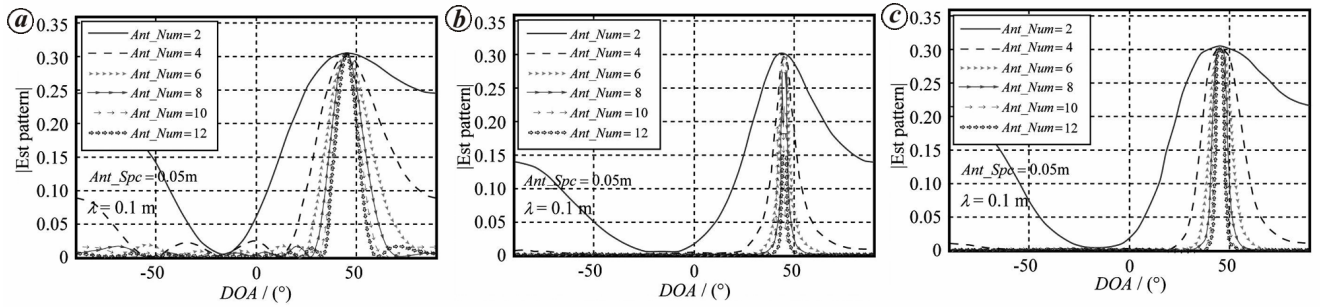


Figure 8. Relationship between $\beta(\theta)$ and (Ant_Num) in three direction of arrival methods. *a*, Least square; *b*, Capon; *c*, amplitude phase estimation.

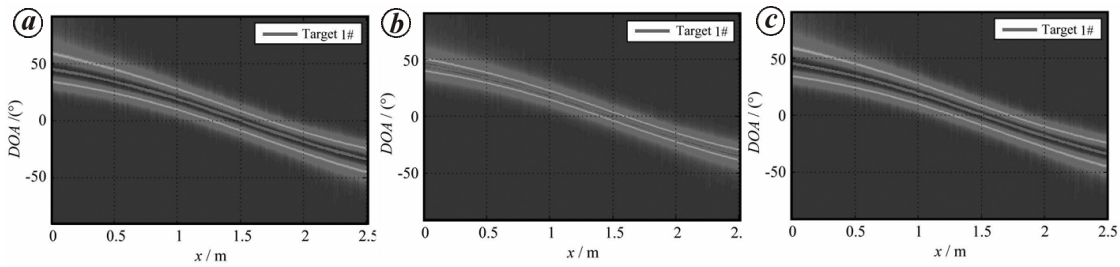


Figure 9. $\beta(\theta)$ in different positions of the measuring line. *a*, Least square; *b*, Capon ; *c*, amplitude phase estimation.

the model in Figure 4. Larger the target angle, higher the precision of DOA estimation in least square and amplitude phase estimation. In the Capon method, the precision of DOA estimation is high in the whole target range.

with $\theta_x = \arctan(x^2 + z^2)$. The imaging point can be drawn as

$$P(x, z) = \sum_x \alpha_x(\theta_x). \tag{26}$$

Inverse direction imaging method

The principle of inverse direction imaging method principle schematic diagram based on DOA estimation is shown in Figure 10. In the 2D model condition, assuming the observed array in the horizontal direction $z = 0$, the target DOA coefficient estimated at the measuring line x is $\alpha_x(\theta)$, whose angle θ changes following $\theta \in \Omega\{\theta\} | -90^\circ \leq \theta \leq 90^\circ\}$. Assuming the imaging position is (x, z) , the target DOA estimation corresponding to the imaging point at the measuring point is $\alpha_x(\theta_x)$,

Single target imaging

As shown in Figure 11, for the simulation parameters of the model, the transmitting and receiving antennas are used in common in uniform linear array with $N_T = N_R = 6$, the antenna element $d = 2.5$ cm, i.e. $\lambda_0/4$, the total array length $L_{Ant} = 5 \times d = 12.5$ cm, the array moving range $X = 0 - 2.5$ m, and with totally 50 measuring points evenly collected. Figure 12 *a-c* shows the imaging results of DOA estimation using least square, Capon and amplitude phase estimation. It is observed that the Capon

algorithm comparatively has a distinctly higher imaging resolution ratio.

Multiple target imaging

The multiple target imaging model is shown in Figure 13, with measuring parameters the same as those in Figure 11. Figures 14–16 show DOA estimation results using the three methods respectively. In a large target spacing, there is reasonable imaging in all three methods. The imaging precision of the two targets in least square is low in resolution compared to the other two methods, with a larger target range. The target amplitude and capacity in amplitude phase estimation are low. For model 2 which has a small target spacing, there are distinct deviations about the position estimation in least square and amplitude phase estimation methods, due to lack of resolution. The imaging in amplitude phase estimation in model 2 is of extremely poor quality; it can only ascertain the existence of two targets in space, but hardly provides the target position.

It is observed in the imaging result of least square that deeper the target, lower is the imaging resolution ratio. This is similar to the result of conventional impulse ground radar detection, but caused due to different reasons. In the conventional impulse ground radar, the background medium has a low-pass filtering action to the

transmitting signal and echo signal, with the signal band width lessened and with high frequency element loss, so that the subwave width is broadened and time resolution is lowered. The echo wave of the deep target receives more low-pass filtering action than the shallow one, and thus has a relatively lower target resolution ratio. This is because DOA estimations for the deep target show little difference at various measuring points, which consequently causes angular vagueness. To enhance the target detection resolution ratio, the field angle φ requires to be widened. The increase of φ facilitates the antenna to measure the target from various directions and from different angles φ . DOA estimations for different measuring points will vary so as to enrich the spatial information for realizing a higher detection precision.

In Figure 17, the two targets are arranged in horizontal direction with different spacings (1 and 0.5 m in models 1 and 2 respectively); the observation parameters are maintained the same as those in the two above-mentioned models.

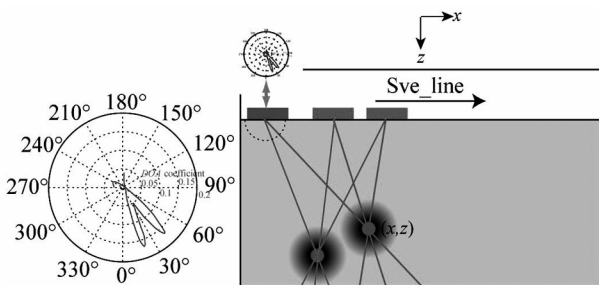


Figure 10. Inverse direction imaging method principle schematic diagram based on direction of arrival estimation.

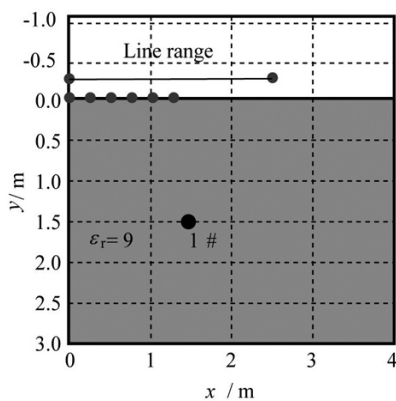


Figure 11. Single target model.

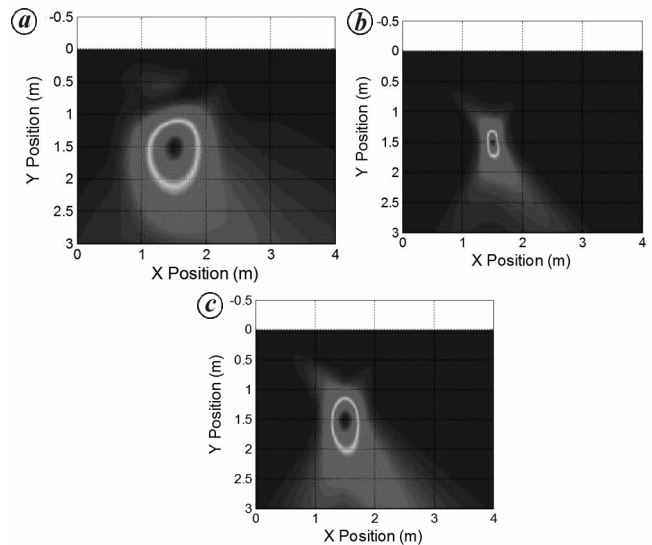


Figure 12. Inverse direction imaging method results. *a*, LS; *b*, Capon; *c*, amplitude phase estimation.

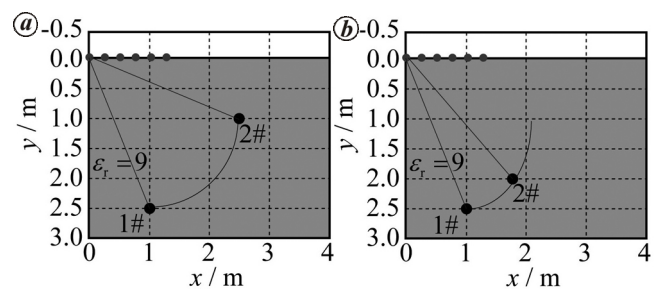


Figure 13. Two-target model equidistant to the array initial position models (*a*) 1 and (*b*) 2.

The DOA estimation results in the three methods are respectively shown in Figures 18–20. The two targets in the model are both underneath the measuring line. Thus the positive–negative angles of DOA at the target surface are observable. So the imaging has a high horizontal resolution. Due to the small field angle of the target measuring line, the vertical resolution ratio in the imaging is low. The horizontal spacing is large between the two

targets in least square due to the different field angles of the array measuring position. The field angle φ in target 1 is negative, thus the image in target 1 stretches and offsets leftwards, while the image in target 2 is just the reverse. Consequently, a large spacing occurs between the two. If there are more targets, it is predicted that when the target spacing reaches 0.5, the precision of DOA in amplitude phase estimation method may be too low to distinguish out the quantity of the targets.

From the simulation and analysis of the above models, it is inferred that the direction of arrival inverse direction imaging method can image the point target reasonably well, by multiple collections in different spatial positions and combining with DOA estimation obtained from array signal scanning. The imaging starts in the model space, scans each imaging point inside, integrates and summarizes the DOA amplitude values estimated in each measuring point, to determine both the target position and

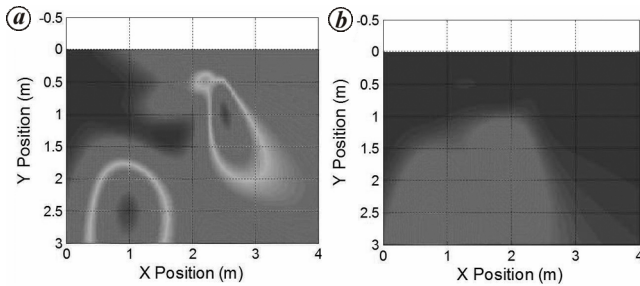


Figure 14. Least square inverse direction imaging method results. *a*, Model 1; *b*, model 2.

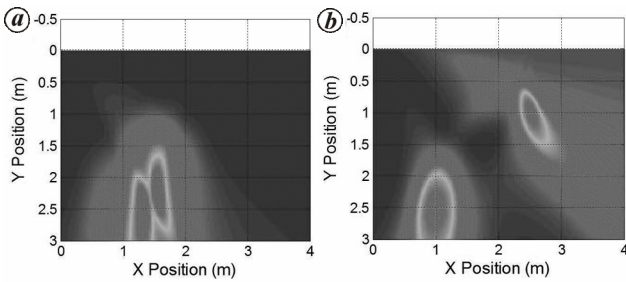


Figure 15. Capon inverse direction imaging method results. *a*, Model 1; *b*, model 2.

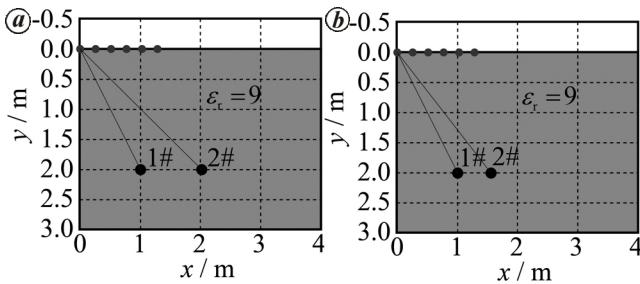


Figure 16. Amplitude phase estimation inverse direction imaging method results. *a*, Model 1; *b*, model 2.

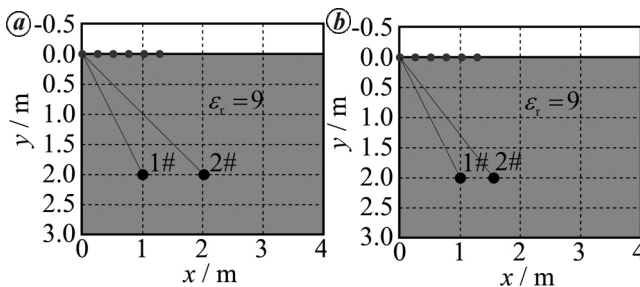


Figure 17. Two-target model with different horizontal spacings. *a*, Model 1; *b*, model 2.

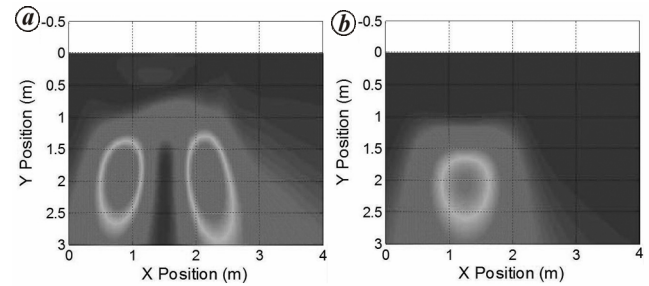


Figure 18. Least square inverse direction imaging method results. *a*, Model 1; *b*, model 2.

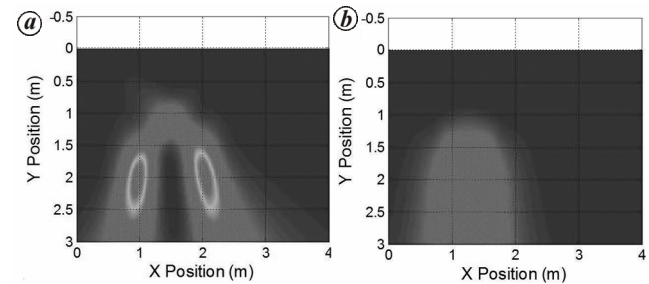


Figure 19. Amplitude phase estimation inverse direction imaging method results. *a*, Model 1; *b*, model 2.

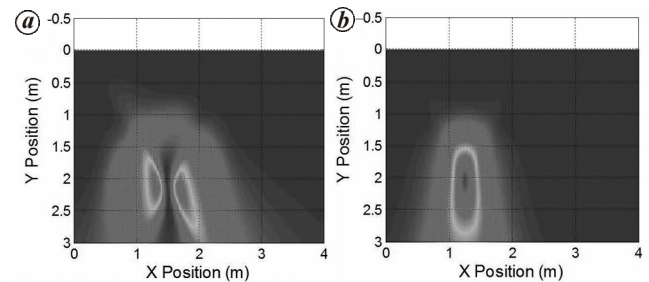


Figure 20. Amplitude phase estimation inverse direction imaging method results. *a*, Model 1; *b*, model 2.

amplitude. This method, with the advantages of simplicity in algorithm and requirement of less observation frequency, improves the measuring speed as well as efficiency of data processing and interpretation.

Summary and conclusion

By comparing the precision of DOA estimation based on adaptive beam-forming and the characteristic of target imaging in least square, Capon algorithm and amplitude phase estimation, we put forward a MIMO-GPR inverse direction imaging method for data processing and target imaging with DOA estimation as the basis. It is observed that the resolution of DOA estimation is higher in the Capon method. The precision does not depend on SNR in least square in the target direction. The estimation performance in amplitude phase estimation falls between least square and Capon. The precision and stability of estimation in the Capon method is high even for a small antenna spacing and array aperture. According to the analysis of narrow-band signal amplitude and phase position, the low pass filtering action and dispersion effect of background medium have an influence on the amplitude of the receiving signal and identification of the phase position, but have little influence on the signal band width. Therefore, the influence on the MIMO-GPR system is substantially weakened, provided that the carrier frequency and transmitting power are appropriate. In the MIMO-GPR inverse direction imaging method system, by spatial scanning of the measuring points for a precise localization of the target, the position parameters with higher precision are worked out and the target detection accuracy is improved. Therefore, the MIMO-GPR inverse direction imaging method can be used in the detection of shallow buried objects like landmines, underground pipelines, etc.

1. Roberts, W. *et al.*, Sparse learning via iterative minimization with application to MIMO radar imaging. *IEEE Trans. Signal Proc.*, 2014, **59**(3), 1088–1101.
2. Xu, L. Z., Li, J. and Stoica, P., Radar imaging via adaptive MIMO techniques. In 14th European Signal Processing Conference, Florence, 2006, pp. 1–5.
3. Tabrikian, J., Barankin bounds for target localization by MIMO radars. In Fourth IEEE Workshop on Sensor Array and Multi-channel Processing, 2006, pp. 278–281.
4. Ju-Ting, W. and Shengli, J., Cramer-Rao bounds of DOA estimation for MIMO radars in compound-Gaussian clutter. *J. Electron. Infor. Technol.*, 2009, **31**(4), 786–789.
5. Wei, X. and Zi-Zhu, H., On the robustness of the APES algorithm in the parameter estimation of MIMO radars. *Acta Electron. Sin.*, 2008, **36**(9), 1804–1809.
6. Xing-Bin, H. *et al.*, An Imaging technique based on distributed multi-channel radars. *J. Electron. Infor. Technol.*, 2007, **29**(10), 2354–2358.
7. Ma, X. Y., Wang, D. W. and Su, Y., High-resolution imaging using a narrowband MIMO radar system. In The 9th International Conference on Signal Processing, Beijing, China, 2008, pp. 2263–2267.
8. Wang, H. J. and Su, Y., Narrowband MIMO radar imaging with two orthogonal linear T/R arrays. In The 9th International Conference on Signal Processing, Beijing, China, 2008, pp. 2513–2516.
9. Ji-Yu, S., Electromagnetic analysis and simulation of MIMO radar imaging. Ph D thesis, Harbin University of Science and Technology, Harbin, China, 2012, pp. 23–33.
10. Jabbarian-Jahromi, M. and Kahaei, M. H., Two-dimensional SLIM with application to pulse Doppler MIMO radars. *Eur. J. Adv. Signal. Process.*, 2015, **2015**, 1–12.
11. Tian-Yun, W., Research on distributed radar sparse imaging technologies, Ph D thesis, University of Science and Technology of China, China, 2015, pp. 3–25.
12. Zeng, Z. *et al.*, Improving target detection accuracy based on multipolarization MIMO GPR. *IEEE Trans. Geosci. Remote Sensing*, 2015, **53**(1), 15–24.
13. Zhao, Y. N. *et al.*, Computational design of optimal waveforms for MIMO radar via multi-dimensional iterative spectral approximation. *Multidimen. Syst. Signal. Process.*, 2014, **27**(1), 1–18.
14. Li, L. and Tian-Shuang, Q., Novel method for joint parameter estimation based on FPSD in wideband bistatic MIMO radar system. *J. Commun.*, 2014, **35**(6), 192–199.
15. Li, N. *et al.*, MIMO radar moving target detection against compound-Gaussian clutter. *Circuits Syst. Signal Process.*, 2014, **33**(6), 1–21.
16. Liu, X. *et al.*, High-resolution swath bathymetry using MIMO sonar system. *J. Syst. Eng. Electron.*, 2014, **25**(5), 761–768.
17. Wei, X., MIMO radar model and the signal processing research. Ph D thesis, Xidian University, Xi'an, 2007, pp. 3–8.
18. Li, J., *MIMO Radar Signal Processing*, John Wiley, New Jersey, USA, 2009, pp. 2–60.
19. Nehorai, A., Storer, D. and Stoica, P., Direction-of-arrival estimation in applications with multipath and few snapshots. *Circuits, Syst. Signal. Process.*, 1991, **10**(3), 327–342.
20. Bo, L., Orthogonal waveform MIMO radar signal design and processing. Ph D thesis, University of Electronic Science and Technology, Chengdu, 2008, pp. 9–30.
21. Fuhnmann, D. R. and Antonio, G. S., Transmit beamforming for MIMO radar systems using partial signal correlation. In 38th Asilomar Conference on Signals Systems and Computers, 2014, vol. 1, pp. 295–299.
22. Donnet, B. J. and Longstaff, I. D., Combining MIMO radar with OFDM Communications. In 3rd European Radar Conference, 2006, vol. 1, pp. 37–40.

Received 6 July 2016; accepted 27 July 2017

doi: 10.18520/cs/v114/i05/1014-1023